

**University of California**  
**Ernest O. Lawrence**  
**Radiation Laboratory**

**SEGMENTED LAMINAR FLOW AND OTHER MODELS  
FOR PACKED-BED LONGITUDINAL DISPERSION**

**TWO-WEEK LOAN COPY**

*This is a Library Circulating Copy  
which may be borrowed for two weeks.  
For a personal retention copy, call  
Tech. Info. Division, Ext. 5545*

## **DISCLAIMER**

This document was prepared as an account of work sponsored by the United States Government. While this document is believed to contain correct information, neither the United States Government nor any agency thereof, nor the Regents of the University of California, nor any of their employees, makes any warranty, express or implied, or assumes any legal responsibility for the accuracy, completeness, or usefulness of any information, apparatus, product, or process disclosed, or represents that its use would not infringe privately owned rights. Reference herein to any specific commercial product, process, or service by its trade name, trademark, manufacturer, or otherwise, does not necessarily constitute or imply its endorsement, recommendation, or favoring by the United States Government or any agency thereof, or the Regents of the University of California. The views and opinions of authors expressed herein do not necessarily state or reflect those of the United States Government or any agency thereof or the Regents of the University of California.

UNIVERSITY OF CALIFORNIA

Lawrence Radiation Laboratory  
Berkeley, California

AEC Contract No. W-7405-eng-48

SEGMENTED LAMINAR FLOW AND OTHER MODELS  
FOR PACKED-BED LONGITUDINAL DISPERSION

Alphonse Hennico, Gabriel Jacques and Theodore Vermeulen

November 16, 1964

SEGMENTED LAMINAR FLOW AND OTHER MODELS  
FOR PACKED-BED LONGITUDINAL DISPERSION

Alphonse Hennico\*, Gabriel Jacques\*, and Theodore Vermeulen

ABSTRACT

For comparison with the diffusion, random-walk, and mixing-cell models of axial dispersion, a segmented-laminar-flow model is developed for packed beds, by analogy with Taylor's derivation for concentration distribution in laminar pipe flow. Two different radial distributions of velocity are assumed, the quadratic profile having its average velocity at one-half the peak value, and a "quartic" profile with the average at one-third the maximum. The latter gives substantially better agreement with experiment, but is still imperfect. A numerical evaluation is described for the concentration distribution, and the results are presented in graphical form. The techniques developed here, when used with an effective velocity distribution still to be determined, are expected to provide a dependable and versatile description of liquid-phase laminar-flow breakthrough behavior.

---

\* Present address: Institut Français du Pétrole, Rueil-Malmaison  
(S-et-O), France.

### Introduction

The subject of lengthwise fluid mixing in continuous-flow packed-column systems has received much attention during the past decade. Several studies have shown that longitudinal dispersion (or "axial mixing") can exert a significant effect in reducing the mass-transfer performance of columns below that predicted from true mass-transfer coefficients alone, and hence, that this effect should be accounted for separately.<sup>24, 34, 38</sup> Several mixing models have been proposed for explaining experimental breakthrough (concentration vs time) data for the outflow. The problem of these models is essentially that of predicting the behavior of an initially sharp interface between two miscible fluids.

The most widely used approach to axial dispersion is the diffusion model. In this model the dispersion process is characterized by a diffusion equation, with an axial-dispersion coefficient in place of the usual molecular diffusivity. A simple solution to the diffusion model, assuming infinite boundary conditions, was first obtained by Danckwerts.<sup>10</sup> The main features of the simple diffusion model were further discussed by several other investigators,<sup>1, 7, 13, 31, 33, 39</sup> but this model does not give an adequate description of axial dispersion in "shallow" beds. An exact analytic solution to the diffusion model, for miscible fluid displacement in beds of finite length, was first presented by Yagi and Miyauchi.<sup>42</sup> Extensive numerical results, based on an asymptotic approximation to this solution, were reported by Brenner.<sup>3</sup>

A second model for axial dispersion, the perfect-mixing cell model, in which each of the interstices of a packed bed acts as a mixing stage, was proposed by Kramers and Alberta.<sup>29</sup> When the series-mixer model was applied to experimental data, it was often found that fewer than ten mixers were needed to reproduce the observed data. Since the beds involved were more than ten packing-particle diameters in length, Carberry suggested that incomplete mixing in the individual

void cells would reduce the calculated number of mixers, relative to the actual number of void cells as indicated by the number of layers of packing.<sup>6</sup> Accordingly, he introduced a mixing-efficiency factor for the series-mixer model, which constituted a free parameter for fitting the model to the experimental data. For "deep" beds (those having 20 or more perfect mixers in series), it has been shown that the diffusion and series-mixer models predict essentially identical residence-time distributions and breakthrough curves.<sup>1</sup>

A random-walk model, developed by Einstein<sup>15</sup> for the stream transport of suspended solid particles, has been extended by Jacques and Vermeulen<sup>23, 24</sup> and Cairns and Prausnitz<sup>5</sup> to the problem of longitudinal dispersion in packed beds. This model, describing the random path of tracer molecules by statistical considerations, also approaches the simple diffusion model at high flowrates. For practical purposes, the random-walk model is numerically equivalent to the diffusion model with finite boundary conditions.

A different statistical model has been investigated by de Josselin de Jong,<sup>26</sup> and analyzed more completely by Saffman.<sup>37</sup> In this model the porous medium is considered as an assembly of randomly oriented straight circular-bore capillary tubes of equal length. The capillary model seems to have two basic defects:<sup>9</sup> A packing of spherical particles has an open-pore structure seemingly not analogous to a capillary structure except perhaps during laminar flow; further, a streamline through the packing does not point in every direction with equal probability, but is strongly weighted toward the average direction of flow.

A number of other models have been proposed in which parallel and series-parallel communication of void cells<sup>14</sup> or material exchange between flowing channels and stagnant pockets of fluid<sup>14, 19, 28</sup> is used to describe dispersion in packed beds. These models include a sufficient number of parameters to allow fitting the model to the available data; they introduce assumptions regarding the frequency of communication of neighboring cells and the relative importance of participating transport mechanisms, which are not usually verifiable

by independent laboratory measurements.

Experimental studies conducted as part of the present investigation indicate that the random-walk and exact diffusion treatments give an excellent fit to the concentration-vs-time curves obtained at higher flow rates, but give a relatively imperfect fit to those for lower flow rates. As shown in the next section, the higher flow rates can be identified with a turbulent-flow regime, and the lower rates with a laminar regime. To meet a need for more detailed study of the laminar regime, a new model is introduced which is statistical in its concept but explicit in its mathematical behavior, being patterned after G. I. Taylor's study of the dispersion effect that results from velocity distribution in laminar flow through cylindrical tubes.<sup>40</sup>

## A. Segmented-Laminar-Flow Model

### 1. Nature of the Laminar-Flow Regime in Packed Beds

Longitudinal-dispersion studies by Jacques and Vermeulen,<sup>23</sup> Carberry and Bretton,<sup>7</sup> and others show the existence of a laminar and a turbulent region with a fairly sharp transition region between them.

When these results are compared with a typical packed-bed friction-factor plot ( $f$  vs  $N_{Re}$ ), where  $N_{Re} = d_p U_0 / \nu$ , with  $d_p$  the equivalent-sphere-volume diameter of the packing material,  $U_0$  the superficial velocity, and  $\nu$  the kinematic viscosity, it is seen that the transition for axial-dispersion occurs in the same Reynolds-number range (see Fig. 1).

A second item of evidence can be found in studies by Garner et al. of the flow pattern around single spheres.<sup>17</sup> In these studies, the following changes in flow pattern with increasing Reynolds number were observed: At first, the flow is entirely streamline and satisfies Stokes's solution. The velocity then begins to decrease on the downstream surface of the sphere, and increases on the upstream surface. The trend continues until separation of the forward flow occurs at  $d_p U_\infty / \nu$  of 15 to 25, when a very small, weak, toroidal vortex is formed near the rear stagnation point. The vortex gains strength as the Reynolds number increases further; the separation ring advances toward the equator, until at  $d_p U_\infty / \nu$  around 450 (with the angle of separation equal to 104 deg) the wake becomes unstable, oscillating about the axis of motion, and spilling its content downstream. Ranz has shown that the interstitial velocity in packed beds is often eight to ten times the superficial

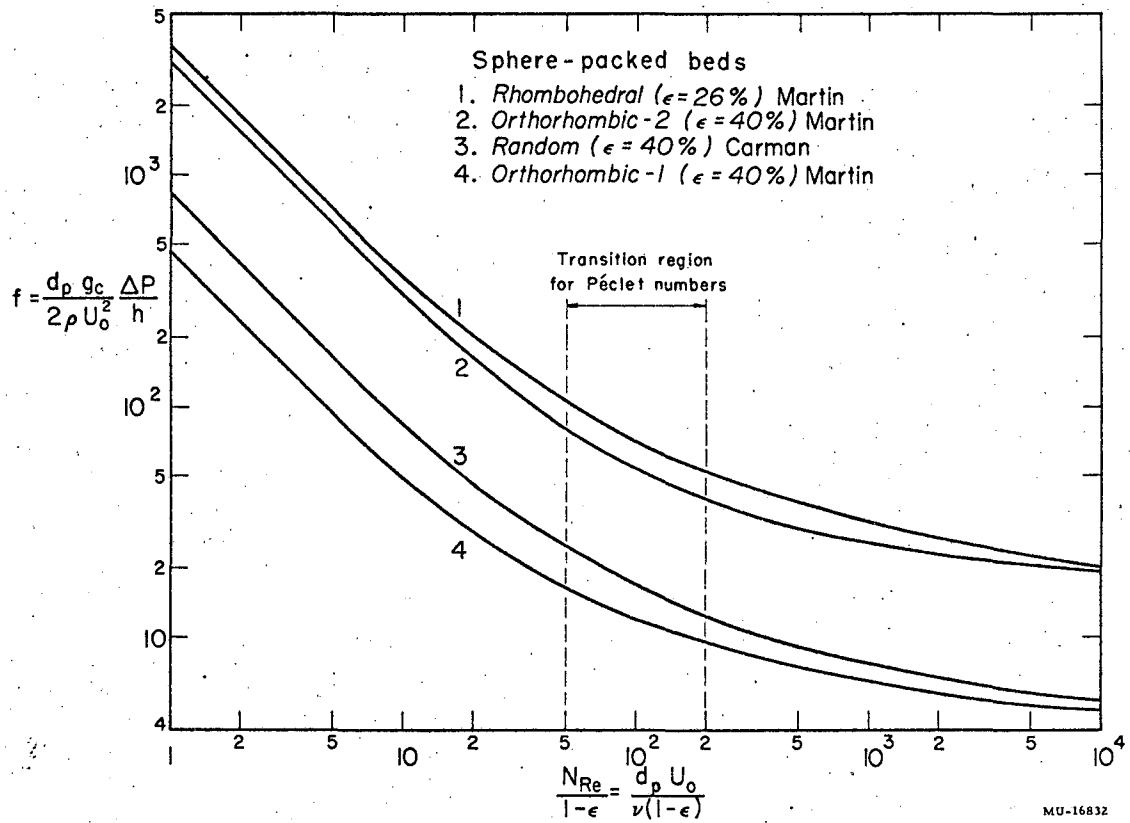


Fig. 1. Friction factor for beds of solids.

velocity, upon which the packed-bed Reynolds number ( $d_p U_0/\nu$ ) is based.<sup>36</sup> The wake instability can be identified with a flow condition in which the flow through a void space in the packing changes from predominantly streamline to near-perfect mixing. In terms of Garner's results, this change should occur at a  $d_p U_0/\nu$  value of around 50 or  $d_p U_0/\nu(1-\epsilon)$  of 80 to 90, where  $\epsilon$  is the porosity.

Using a suspension of fine particles to indicate the fluid motion, Hiby has cited photographic evidence of the transition from turbulent to laminar flow in packed beds; below  $N_{Re} = 10$ , completely laminar flow was observed.<sup>21</sup>

A somewhat different investigation, dealing with liquid flow in a falling film over a single-file column of spheres in contact, also shows evidence for a laminar-turbulent flow transition.<sup>11</sup>

Experimental evidence for the presence of a laminar-turbulent transition region has also been found in heat- and mass-transfer studies. Gamson and coworkers derived the following two relations for the Colburn  $j$  factor in mass-transfer:<sup>16</sup>

$$j_d = 1.46 N_{Re}^{-0.41} (1-\epsilon)^{0.65} \text{ for } \frac{N_{Re}}{1-\epsilon} > 100,$$

and

$$j_d = 17 N_{Re}^{-1} (1-\epsilon)^{1.2} \text{ for } \frac{N_{Re}}{1-\epsilon} < 100.$$

Due to experimental uncertainties, and perhaps also due to the gradual nature of the transition, the exact occurrence of the breakpoint is not well known.

From the various indications, considerable justification exists for dividing the axial-dispersion phenomena into two different regions separated by a critical value (or range of values) of the Reynolds number.

## 2. Description of the Model

As just mentioned, the laminar regime of packed-bed flow (in columns having relatively uniform mean flow through all cellular elements of any one cross section--e. g., in circularly cylindrical columns) requires further study in order to obtain a physical model that will correspond accurately to the experimental outflow-concentration histories (or breakthrough curves). A new model, which constitutes a step in this desired direction, is termed "segmented laminar flow."

In the actual laminar-flow behavior of a column, each fluid filament undergoes changes in velocity from point to point along its path. Such filaments can be considered to enter a new column "segment" each time their velocity crosses the mean velocity of the fluid. If the distribution of velocities is the same at each cross-section, as in randomly packed beds, one or more other filaments will be reduced in velocity at the cross section where a particular filament changes from a slow-moving to a fast-moving segment/ (Fig. 2a). The resulting interchange of fast-moving and slow-moving segments is equivalent to gradual but continual remixing of filaments. In the idealized model postulated here, this gradual mixing is replaced by a sequence of cross-sections at uniform intervals, where complete mixing occurs, with complete absence of mixing at intermediate points/ (Fig. 2b). The interval between the mixing cross-sections becomes equivalent to a weighted average of the actual segment lengths. In each segment then, laminar flow occurs with well defined velocity profiles, and transverse molecular diffusion is treated as negligible.

In this study, two different velocity profiles are used. One is the familiar quadratic (parabolic) profile,  $u/u_{\max} = 1 - (r/R)^2$ , where  $u$  is the mean local velocity of a flow filament, and  $r/R$  is the mean ratio of its radius to the total radius of the passage. The other one, which we call "quartic," has the empirical form  $u/u_{\max} = [1 - (r/R)^2]^2$ . While the quadratic velocity distribution might fit the flow through a bundle of parallel circular-bore tubes, the quartic distribution appears to provide a more accurate description of packed-bed flow, in the laminar regime.

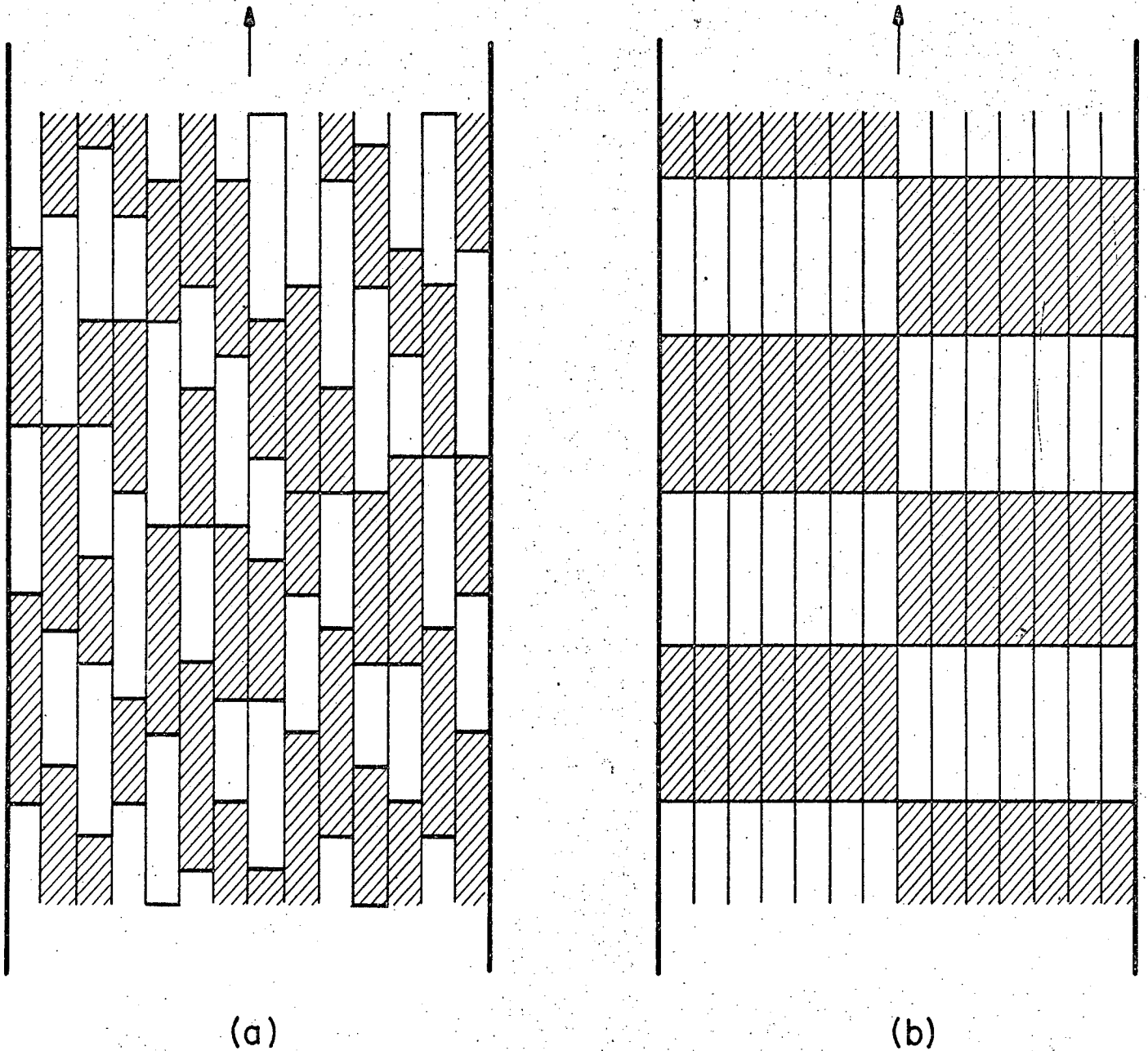


Fig. 2. Idealized flow filaments, showing points of interchange between low-velocity (unshaded) and high-velocity (shaded) segments. (a) Random distribution. (b) Simplified model with uniform spacing of segments.

MU-31815

At the end of each segment the liquid is assumed to be thoroughly mixed before it enters the next segment. Mathematically, a flow-average "cup-mixing" composition is computed after each segment, which represents the composition of the feed to the following segment.<sup>2, 25</sup> The boundary condition at the column inlet corresponds to a step-input of a tracer material. The exact solution is not obtainable for the response curve after each segment, but a numerical solution has been derived by digital computation. The resulting theoretical breakthrough curves for different numbers of segments can be fitted to the individual experimental breakthrough curves. Each experimental run will thus exhibit a "number of dispersion units" which can be considered as a "column Péclet number";  $N = h/\ell$  or  $hU_0/E$ , for purposes of defining an effective axial dispersion coefficient (here  $h$  is column height,  $\ell$  is mixing length,  $U_0$  is superficial velocity, and  $E$  is the superficial dispersion coefficient). From this, a "packing Péclet number",  $P = d_p/\ell$  or  $d_p U_0/E$ , is calculated which presumably is constant over the entire length of the packed bed.

### 3. General Mathematical Approach

The equations were derived for a cylindrically symmetrical element of flow path having the cross-section  $S$ . The flow is assumed unidirectional. The concentration is a function of time  $t$ , of distance in the direction of flow  $z$ , and of a radius vector  $\vec{r}$  which characterizes an element  $dS$  of the cross-sectional area. The local velocity is also a function of  $\vec{r}$  as mentioned above. The flow-average concentration leaving one segment is taken as the feed concentration for the next segment. This flow-average concentration is defined as

$$c_b(z, t) = \frac{\int_S c(\vec{r}, z, t) u(\vec{r}, t) dS}{\int_S u(\vec{r}, t) dS} \quad (1)$$

At each of the cross sections where mixing occurs, the  $\vec{r}$ -dependent concentration is replaced by its bulk average; i. e.,  $c(\vec{r}, z, t)$

is replaced by  $c_b(z, t)$ . In a cylindrical element of flow path (one with uniform cross section) the velocity profile is only a function of  $\vec{r}$ . For steady-state laminar flow, the concentration  $c(\vec{r}, z_k, t)$  at a point  $z_k$  gives directly the concentration at a downstream point,  $z > z_k$ , in the corresponding radial location. Thus we have

$$c(\vec{r}, z, t) = c(\vec{r}, z_k, t - t_1), \quad (2)$$

where  $t_1$  is the time necessary for the fluid to travel the distance  $(z - z_k)$ , and

$$t_1 = \int_{z_k}^z \frac{dz}{u(\vec{r}, t)} = \frac{z - z_k}{u(\vec{r})}. \quad (3)$$

In physical terms, the element of fluid observed earlier at  $z$  is the same as one which was observed earlier at  $z_k$ .

From these relations the general equation for a segment extending from  $z_k$  to  $z_{k+1}$  becomes

$$c_b(z_{k+1}, t) = \frac{\int_S c_b \left[ z_k, t - \frac{z_{k+1} - z_k}{u(\vec{r})} \right] u(\vec{r}) dS}{\int_S u(\vec{r}) dS}. \quad (4)$$

In this study, the problem is analyzed with reference to a fluid in a circularly cylindrical volume element of radius  $R$ . For this case, Eqs. (1) and (4) become

$$c_b(z, t) = \frac{\int_0^R u(r) c(r) r dr}{\int_0^R u(r) r dr} \quad (5)$$

and

$$c_b(z_{k+1}, t) = \frac{\int_0^R c_b \left( z_k, t - \frac{z_{k+1} - z_k}{u(r)} \right) u(r) r dr}{\int_0^R u(r) r dr}. \quad (6)$$

By use of these equations, it is possible in principle to compute the

concentration of tracer material after any number of segments, if one knows the velocity distribution and the concentration distribution at the inlet as a function of time and position. In practice, the multiple integration required for successive segments becomes progressively more complex, and soon ceases to give relations in closed analytical form. The separate application of these basic equations to the quadratic and quartic velocity profiles is given in the following sections.

#### 4. Quartic Velocity Distribution

A major result of the quadratic velocity profile is that it takes at least half of the stoichiometric time before any breakthrough sets in. This is unrealistic physically; many experimental curves start earlier, or have shapes that would correspond to less than one segment. The reason for this partial failure of the quadratic model is believed to lie in the assumption of a circular shape for the flow element, in which the maximum fluid velocity is twice the average velocity. In reality the packing voids have a curved triangular, rectangular, or still more complex shape, with corners in which the fluid is practically stagnant. This tends to lead to an average fluid velocity smaller than half of the maximum, and in turn frequently to breakthrough-curve slopes smaller than those given by the quadratic distribution. As no exact expression for the velocity profile in these complex voids is available, an empirical relation giving  $(u_{\max}/U)=3$  has been adopted as a convenient and reasonable starting point.

The expression for the quartic velocity profile is

$$\frac{u(r)}{u_{\max}} = \left(1 - \frac{r^2}{R^2}\right)^2 \quad (7.)$$

where  $u_{\max}$  is the maximum velocity of the fluid and  $r$  is a radial coordinate.

From Eq. (7), the flow-average concentration is given by

$$c_b = \frac{6}{R^2} \int_0^R c(r) \left[1 - \frac{r^2}{R^2}\right]^2 r dr \quad (8)$$

This relation can be simplified by the following change of variable:

$$\zeta = 1 - \frac{r^2}{R^2} \quad (9)$$

here also

$$\zeta = \left( \frac{u}{u_{\max}} \right)^{1/2} \quad (10)$$

$\zeta$  is thus the fraction of area enclosed between  $r$  and  $R$ . Differentiation gives

$$d\zeta = - \frac{2r \, dr}{R^2} \quad (11)$$

The integration limits are at  $r = 0$ ,  $\zeta = 1$ , and at  $r = R$ ,  $\zeta = 0$ . Applying these relations to the segment  $(z_k, z_{k+1})$  leads to the more specific relation

$$c_b(z_{k+1}, t) = 3 \int_0^1 \left[ c_b \left( z_k, t - \frac{z_{k+1} - z_k}{u_{\max} \zeta^2} \right) \right] \zeta^2 \, d\zeta \quad (12)$$

Equation (12) proves to be the key expression for evaluating the concentration breakthrough after any given number of segments. Applied to a column of total length  $h$ , divided into a number of segments  $N$ , each of length  $\ell$ , it becomes

$$c_b(z_N, t) = 3 \int_0^1 \left[ c_b \left( z_{N-1}, t - \frac{z_N - z_{N-1}}{u_{\max} \zeta^2} \right) \right] \zeta^2 \, d\zeta \quad (13)$$

The initial condition can be described by the relation

$$c(0, r; t) = c_b(0, t) = c_0 H(t), \quad (14)$$

where  $c_0$  is the step-input concentration, and  $H(t)$ , the Heaviside unit function, is either zero or unity, depending on whether its argument is smaller or larger than zero. The Heaviside function expresses the fact that the tracer fluid takes a well defined time to emerge from the column.

After  $N$  divisions each of length  $\ell$ , the remixed concentration is

$$\begin{aligned} c_b(N\ell, t) &= c_0 f_N(t) \cdot H\left(t - \frac{N\ell}{u_{\max}}\right) \\ &= c_N(t) \cdot H\left(t - \frac{N\ell}{3U}\right), \end{aligned} \quad (15)$$

where  $f_N(t)$  is a dimensionless function of  $t$  that remains to be de-

rived,  $c_N(t)$  is the corresponding concentration  $[= c_0 f_N(t)]$ , and  $U$  is the average linear velocity which for this case is equal to one-third the maximum velocity  $u_{\max}$ . The Heaviside function in the above expression states that  $c_b(Nl, t)$  is nonzero only if  $t \geq Nl/3U$ . Suppose  $c_{N-1}$  is known after  $N-1$  segments; then, at the end of  $N$  segments,

$$c_N(\theta) = 3 \int_0^1 \left[ c_{N-1} \left( \theta - \frac{1}{3\zeta^2} \right) \right] \cdot H \left[ \theta - \left( \frac{N-1}{3} \right) - \frac{1}{3\zeta^2} \right] \zeta^2 d\zeta \quad (16)$$

where  $\theta = Ut/l$ .

In the use of this relation, the argument of the Heaviside function serves to define a new lower limit of integration. Physically, the use of this function means replacing the lower limit by a quantity that avoids computing any negative concentration values. Thus, if we have

$$\theta - \left( \frac{N-1}{3} \right) - \frac{1}{3\zeta^2} > 0, \text{ or } \zeta \geq (3\theta - N + 1)^{-1/2},$$

then

$$H \left[ \theta - \left( \frac{N-1}{3} \right) - \frac{1}{3\zeta^2} \right] = 1, \quad (17)$$

The general relation now becomes

$$X_N(\theta) = 3 \int_{(3\theta - N + 1)^{-1/2}}^1 \left[ X_{N-1} \left( \theta - \frac{1}{3\zeta^2} \right) \right] \zeta^2 d\zeta \quad (18)$$

where  $X_N(\theta) = c_b(Nl, \theta)/c_0$  and similarly for  $X_{N-1}$  at its respective position and dimensionless time; with  $X_N(\theta) = 0$  for  $\theta \leq N/3$ . These equations show that for each added segment,  $\theta$  is replaced by  $\theta - (1/3\zeta^2)$ , and the integration is then performed as indicated.

In dimensionless units,  $X$  can be given as a function of  $N, \theta$ , and  $\zeta$ ; or as a function of  $N, T$ , and  $\zeta$ , where  $T_N = \theta/N$ .\* For the latter case, the integrand function  $X_{N-1}$  is known in terms of  $T_{N-1}$ , but here one wishes to evaluate it in terms of  $T_N$ . This is equivalent to reducing the length of a column of  $(N-1)$  segments from the constant value  $h$  to a new value  $h' = (N-1)h/N$ ; then an extra segment is added to restore the column to length  $h$ . By use of the general definition  $T = \theta/N$  we have

$$T_{N-1} = \frac{\theta}{N-1} - \frac{1}{3\zeta^2(N-1)}, \text{ with } T_N = \frac{\theta}{N} \quad (19)$$

\* For any value of  $N$ , the true filling time for the bed will occur at  $T = 1$ .

Hence

$$X_{N-1}(T_{N-1}) = X_{N-1} \left[ \frac{T_{N-1}^N}{N-1} - \frac{1}{3\zeta^2(N-1)} \right], \quad (20)$$

and Eq. (18) takes the form

$$X_N(T_N) = 3 \int_{[N(3T_N-1)+1]^{-1/2}}^1 \left\{ X_{N-1} \left[ \frac{T_N^N}{N-1} - \frac{1}{3\zeta^2(N-1)} \right] \right\} \zeta^2 d\zeta \quad (21)$$

The relations rapidly become very complex, and an exact solution seems to be impossible for  $N > 2$ . The solution must therefore be found by numerical methods on a high-speed digital computer.

a. Analytic relations. The expressions for beds consisting of only one or two segments can be derived analytically, and will now be given. Their mathematical form is of interest to show the complexity that is reached for beds with a larger number of segments, and also to indicate possible forms of empirical equations for representing the latter.

For  $N = 1$ , Eq. (18) becomes

$$X_1(\theta) = 3 \int_{(3\theta)^{-1/2}}^1 \left[ X_0 \left( \theta - \frac{1}{3\zeta^2} \right) \right] \zeta^2 d\zeta \quad (22)$$

Here  $X_0$ , the value of inlet concentration, is constant at unity. From this,

$$X_1(\theta) = \left[ 1 - (3\theta)^{-3/2} \right] \cdot H \left( \theta - \frac{1}{3} \right) \quad (23)$$

This relation shows that  $X_1(\theta)$  is zero as long as  $\theta \leq 0.33$ . We recall that  $\theta = Ut/l$ , where  $l$  is the length of one segment,  $t$  is the elapsed time, and  $U$  is the mean linear velocity. (no 11)

If  $N = 2$ , the column consists of two segments of equal length. The mixing effluent from the first segment has the concentration  $X_1$ , as just derived. Then,

$$X_2(\theta) = 3 \int_{(3\theta-1)^{-1/2}}^1 \left[ 1 - \left( 3\theta - \frac{1}{\zeta^2} \right)^{-3/2} \right] \zeta^2 d\zeta \quad (24r)$$

This relation is obtained by replacing  $\theta$  by  $[\theta - (1/3\zeta^2)]$  in the expression for  $X_1$ , and by changing the lower limit to avoid computing negative concentration values. Integration of Eq. (24) between the specified limits yields

$$X_2(\theta) = \left[ 1 - \frac{2(3\theta)^3 + 6(3\theta)^2 - 24(3\theta) + 16}{(3\theta)^3 (3\theta - 1)^{3/2}} \right] \cdot H\left(\theta - \frac{2}{3}\right). \quad (25)$$

The argument of the Heaviside function indicates that  $X_2$  is zero for  $\theta \leq 1$ . In terms of  $T$  the equation for  $X_2$  is of identical form but with  $\theta$  replaced by  $2T$  throughout.

### 5. Quadratic Velocity Distribution

It is of interest to examine also the analytic and numeric results for the quadratic profile, despite its apparent inapplicability to packed-column dispersion. The derivation follows an entirely parallel course to the preceding one, but starts with the conventional parabolic relation:

$$\frac{u(r)}{u_{\max}} = 1 - \frac{r^2}{R^2} = \zeta \quad (7a)$$

The relation between the mixed concentration entering segment  $N$  and the remixed concentration leaving it becomes

$$c_b(z_N, t) = 2 \int_0^1 \left[ c_b \left( z_{N-1}, t - \frac{z_N - z_{N-1}}{u_{\max} \zeta} \right) \right] \zeta d\zeta. \quad (13a)$$

Hence

$$X_N(\theta) = 2 \int_0^1 \frac{1}{(2\theta - N + 1)^{-1}} \left[ X_{N-1} \left( \theta - \frac{1}{2\zeta} \right) \right] \zeta d\zeta, \quad (18a)$$

or

$$X_N(T_N) = 2 \int_0^1 \frac{1}{[N(2T_N - 1) + 1]^{-1}} \left\{ X_{N-1} \left( \frac{T_N}{N-1} - \frac{1}{2\zeta(N-1)} \right) \right\} \zeta d\zeta. \quad (21a)$$

The analytic result for the first segment ( $N = 1$ ) is

$$X_1(\theta) = \left( 1 - \frac{1}{4\theta^2} \right) \cdot H(\theta - 0.5) \quad (23a)$$

with  $H(\theta - 0.5)$  unity if  $\theta \geq 0.5$ , and zero if  $\theta < 0.5$ . For  $N = 2$ , the explicit relation is:

$$X_2(\theta) = \left\{ 2(\theta-1) \left[ \frac{(2\theta)^3 + (2\theta)^2 - 6}{(2\theta)^3 (2\theta - 1)} \right] - \frac{12}{(2\theta)^4} \ln(2\theta - 1) \right\} H(\theta - 1). \quad (25a)$$

## 6. Numerical Methods of Solution

For both velocity profiles, the integrations required for successive segments (beyond  $N = 2$ ) were computed by two different numerical methods. In Method 1 we evaluate the integral by a summation scheme using the exact concentration values calculated for the previous segment. This method is quite accurate, but very time-consuming because of its use of a time scale with a constant increment which corresponds to a progressively smaller  $\Delta T$  as  $N$  increases. In Method 2 we evaluate the integral by Simpson's integration formula, getting the necessary concentration values by interpolation among the values calculated for the previous segment. This method is based on the  $T$  scale, and computes the minimum number of concentration values necessary to go up to a specified maximum  $N$ ; it is very fast but becomes unstable for large values of  $N$ . It seems possible that an optimum method would be obtained by combining the favorable features of the two methods, but this has not been done.

In this section, these two methods are explained, using the quartic velocity profile for illustration. Results obtained for both velocity distributions are then given.

a. Method 1. This method numerically solves the analytical expression

$$X_N(\theta) = 3 \int_{(3\theta - N + 1)^{-1/2}}^1 \left[ X_{N-1} \left( \theta - \frac{1}{3\zeta^2} \right) \right] \zeta^2 d\zeta, \quad (26)$$

with

$$\theta = \frac{Ut}{l} = \frac{Ut}{h} N.$$

For ease of computation, a new time variable  $\tau$  is introduced, for which all the curves begin at  $\tau = 0$ . The appropriate transformation is

$$\tau = 3\theta - N = N(3T - 1). \quad (27)$$

Physically,  $\tau = 0$  corresponds to the time of arrival (at the outflow) of the maximum-velocity flow filament, for which  $\zeta = 1$ . When the X-vs-time behavior of a bed length corresponding to  $N$  segments is evaluated from that of a length corresponding to  $N - 1$  segments, the values of  $\tau$  (and  $\theta$ ) used are based upon length  $N$  rather than upon length  $(N-1)$ .

Hence, when  $\tau = 0$  for the evaluation of  $X_N$ , the function of  $\tau$  at which  $X_{N-1}$  is evaluated (which can be termed  $\tau_{N-1}$ ) must also be zero when  $\zeta = 1$ . To state the problem another way, Eq. (27) can be extended to give

$$\tau_{N-1} = \tau_N + 3(\theta_{N-1} - \theta_N) - [(N-1) - N]. \quad (28)$$

From Eq. (26),  $\theta_{N-1}$  is seen to be  $\theta_N - [1/(3\zeta^2)]$ . Hence, we obtain

$$\tau_{N-1} = \tau_N - \frac{1}{\zeta^2} + 1. \quad (29)$$

A test of this relation shows that it does satisfy the condition stated above ( $\tau_{N-1} = 0$  when  $\zeta = 1$ ).

To eliminate subscripts, the function  $\tau_{N-1}$  will be redefined as a time variable  $W$ . Equation (26), the general formula, thus becomes

$$\begin{aligned} X_N(\tau) &= 3 \int_{1/\sqrt{\tau+1}}^1 \left[ X_{N-1} \left( \tau+1 - \frac{1}{\zeta^2} \right) \right] \zeta^2 d\zeta \\ &= \int_{1/\sqrt{\tau+1}}^1 X_{N-1}(W) \zeta^2 d\zeta. \end{aligned} \quad (30)$$

Method 1 involves approximating this integral by a summation, using directly the  $X$  values computed from the previous segment, with the corresponding  $\zeta$  values as shown below. A time increment  $\delta$  is selected such that

$$\tau = m\delta \quad (31)$$

and

$$W = m'\delta, \quad (32)$$

where  $m$  and  $m'$  are integers. From the definition of  $W$ , we have

$$\zeta = (1 + \tau - W)^{-1/2} = [1 + (m - m')\delta]^{-1/2} \quad (33)$$

with  $m \geq m'$ ,  $\zeta$  can take on an infinite sequence of values starting at unity and tending toward zero. The general equation, in summation form, becomes

$$\begin{aligned} X_N(\tau) &= 3 \sum_{m'=0}^{m'=m-1} [X_N(W)]_{av} (\zeta^2)_{av} \Delta\zeta \\ &= 1.5 \sum_{m'=0}^{m'=m-1} [X_N(W)]_{av} (\zeta_{m'}^2 + \zeta_{m'+1}^2) (\zeta_{m'} - \zeta_{m'+1}) \end{aligned} \quad (34)$$

Illustration of the use of these equations is given in Fig. 3.

b. Method 2. Here the dimensionless time scale  $T = \theta/N$  is used directly, time being thus referred to the total length of the column rather than to the length of the individual segments. The general formula used in Method 2 is Eq. (21a):

$$X_N(T) = 3 \int_0^1 [N(3\zeta^2 - 1) + 1]^{-1/2} \left\{ X_{N-1} \left[ \frac{N}{N-1} T - \frac{1}{3(N-1)\zeta^2} \right] \right\} \zeta^2 d\zeta \quad (35)$$

For simplification, a new variable  $V$  is defined as

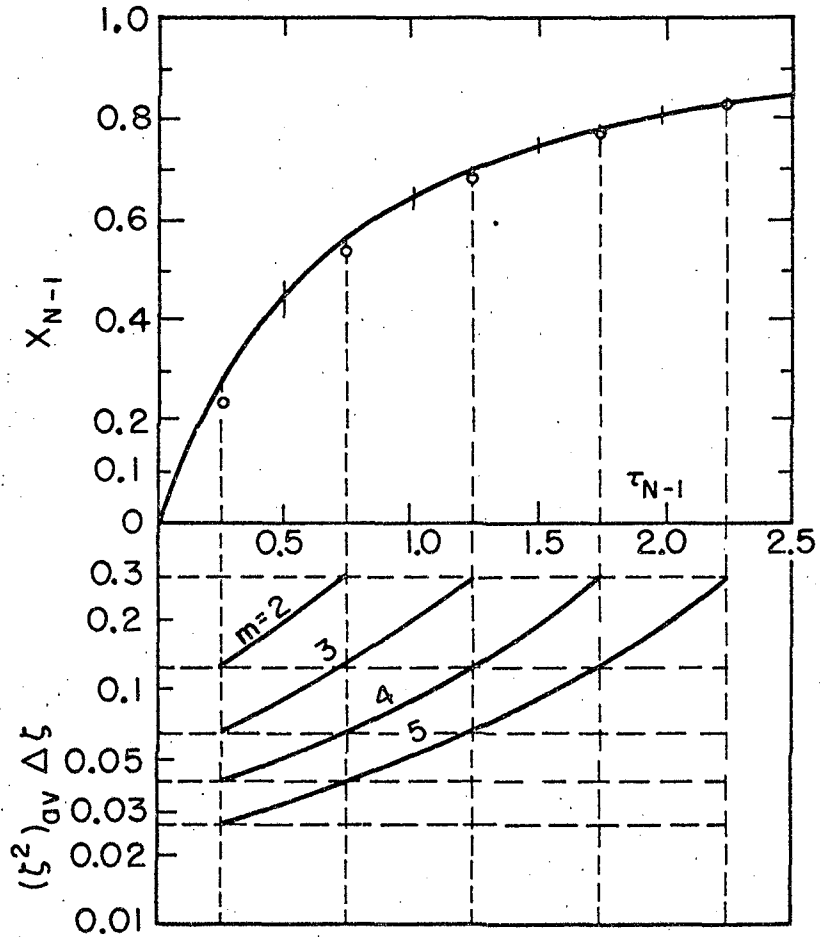
$$V = \frac{N}{N-1} T - \frac{1}{3(N-1)\zeta^2} \quad (36)$$

From this, we have

$$\zeta = [3NT - 3(N-1)V]^{-1/2} \quad (37)$$

and

$$X_N(T) = 4.5 \int_{1/3}^{\frac{3N-1}{3(N-1)}} X_{N-1}(V) \frac{(N-1)}{[3NT - 3(N-1)V]^{2.5}} dV \quad (38)$$



MU-30162

Fig. 137. Illustration of Method 1 for numerical integration.

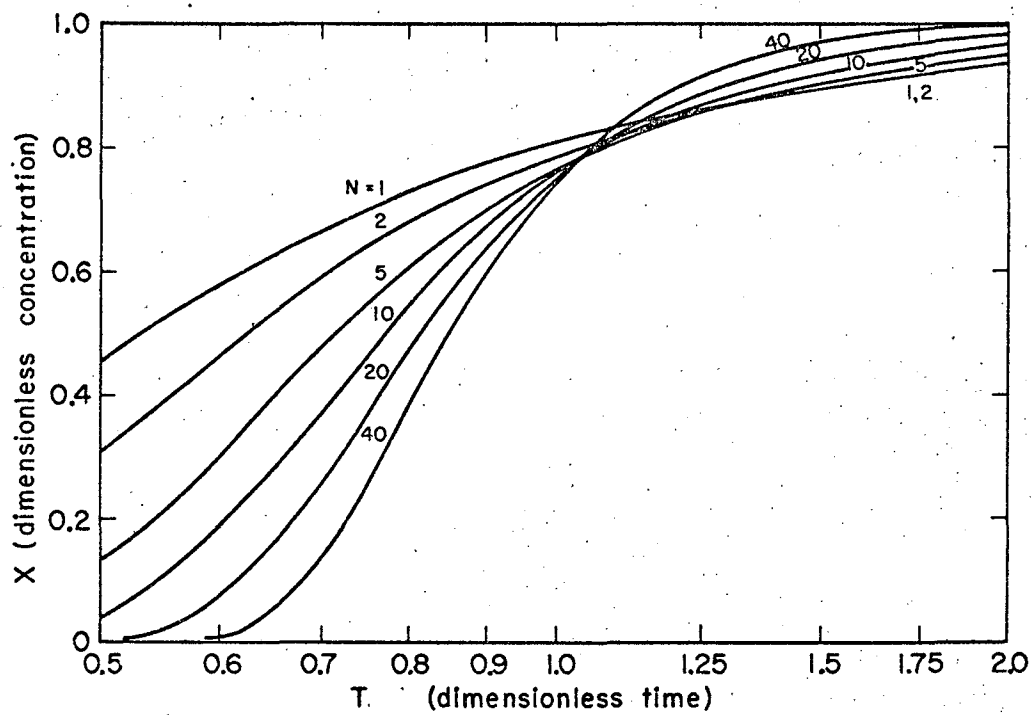
To compute the concentration values  $X_N$  to a dimensionless time value  $T_N$ , it is necessary to know  $X_{N-1}$  values to a time  $T_{N-1}$  larger than  $T_N$ . The relation between the different time values is

$$T_{N-i} = T_N + \frac{i}{N-i} \left( T_N - \frac{1}{3} \right), \quad (39)$$

where  $i$  is an integer. After the largest  $T$  that is needed for the largest  $N$  has been specified, Eq. (39) indicates the largest  $T$  that must be carried for each lesser number of segments.

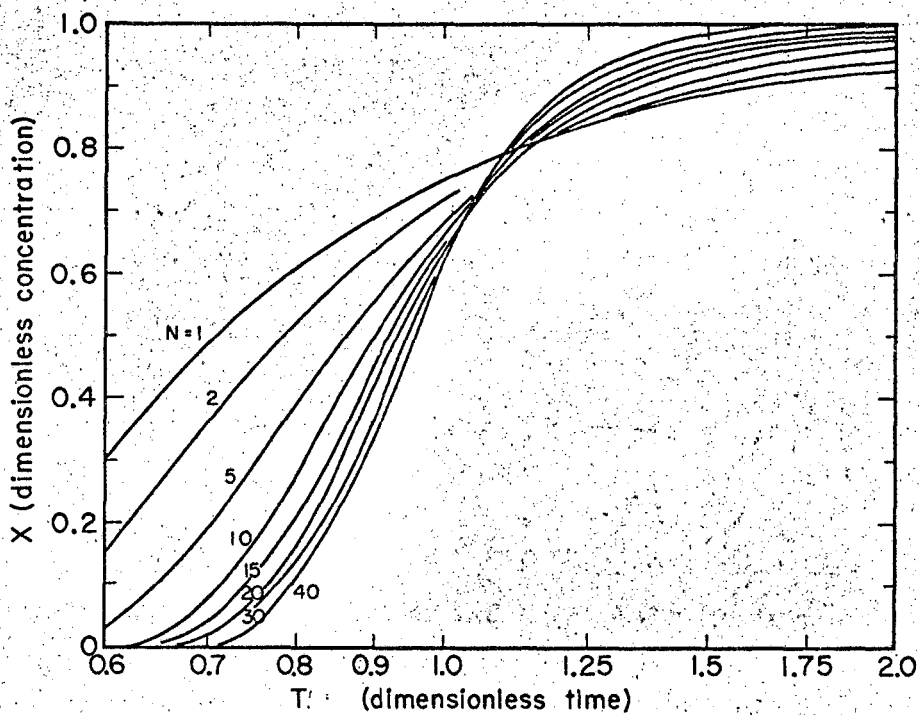
Computation was made with the analytic results for  $N=2$  as starting values. In the computation for each new  $N$ ,  $T$  was varied by constant increments up to the limit. For each  $T$ , Eq. (38) was evaluated by Simpson's integration rule, with the  $X$  values for a specified value of the argument  $V$  being obtained by interpolation. The number of points used in Simpson's rule was determined by specifying the maximum interval between any two successive points on the time scale.

c. Results. Numerical results for the quadratic and the quartic distribution obtained by Method 1 with  $\delta$  (quadratic) = 0.100 and  $\delta$  (quartic) = 0.1667 are given respectively in Figs. 4 and 5, as semi-logarithmic plots of  $X$  vs  $T$ , the time scale being normalized by the stoichiometric time. The numerical results were limited to  $N \leq 45$ , due to the relatively large amount of computer time involved in going further (about 0.5 hr on the IBM 7090 was required for the present range of values). An exact estimate of the error involved in the use of Method 1 is not possible; however, trial runs for the quartic distribution up to  $N = 10$  showed that by reducing the increment  $\delta$  from 0.1667 to 0.0833 the  $X_{10}$  values changed only by 1 digit in the third place. Concentration



MU-30167

Fig. 5. Breakthrough curves for the segmented-laminar-flow model with quartic velocity profile.



MU-30168

Fig. 4. Breakthrough curves for the segmented-laminar-flow model with quadratic velocity profile.

values calculated by Method 2 with  $\Delta V = 0.042$  up to  $N = 10$  did not differ more than 2 digits in the third place from those computed by Method 1. Beyond  $N = 10$ , cumulative errors led to erroneous results unless  $\Delta V$  was much further reduced, which in turn was very time-consuming.

The coordinates of Figs. 4 and 5 are very convenient for comparing experimental breakthrough curves with the theoretical results, since a logarithmic scale of the experimental volume or time will only differ from the logarithm of dimensionless time by a constant additive term.

A frequency-response analysis for the quadratic velocity distribution, obtained from the step-input response, is given elsewhere.<sup>20</sup> A similar approach could be used for the quartic velocity distribution, if needed.

### C. Diffusion Model

In the diffusion model for longitudinal dispersion, it is assumed that equations of exactly the same form apply as those describing the molecular-diffusion process. The governing equation is

$$\frac{E}{\epsilon} \frac{\partial^2 c}{\partial z^2} - \frac{U_0}{\epsilon} \frac{\partial c}{\partial z} = \frac{\partial c}{\partial t}, \quad (40)$$

where  $z$  is axial distance,  $t$  is time,  $c$  is the solute concentration of interest,  $E$  is the superficial axial-dispersion coefficient,  $\epsilon$  is the void fraction, and  $U_0$  is the superficial velocity of the fluid. The solution to this equation has been given for two different sets of boundary conditions corresponding to a finite-length column and to an infinite column.

1. Finite-Length Column (Bounded Diffusion)

An exact solution for the diffusion equation, Eq. (40), applied to a column of finite length, has been given by Yagi and Miyauchi.<sup>42</sup> Brenner has shown that the general equation and the boundary conditions are similar to those governing heat loss to "sinks" at the ends of a slab,<sup>3</sup> for which Carslaw and Jaeger have given the general solution.<sup>8</sup>

The variables in Eq. (40) will be made dimensionless by introducing the relations  $N = h/l = h U_0/E$ ,  $X = c/c_0$ ,  $\theta = U_0 t/l\epsilon$ , and  $Z = z/h$ . Here  $N$  is/a "column Péclet number," or total number of "dispersion units."



The solution,  $X$  at the exit of the column, has the form

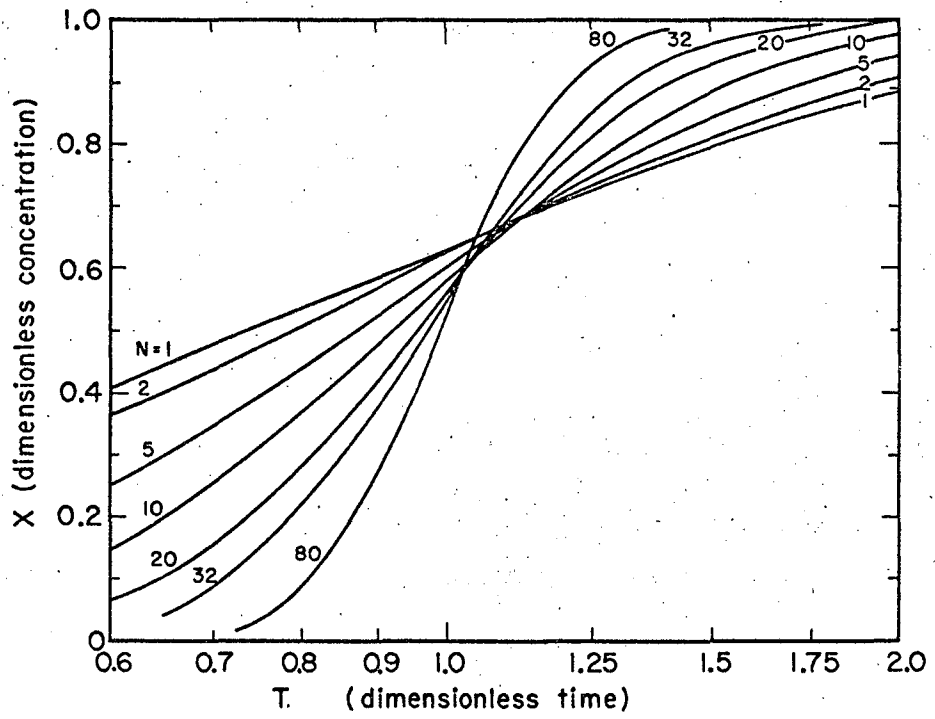
$$X(\theta) = \sum_{n=1}^{n=\infty} \exp\left\{\frac{N}{2} \left[1 - \frac{\theta}{2N} \left(1 + \frac{4\mu_n^2}{N^2}\right)\right]\right\} \quad (41)$$

$$\frac{N\mu_n (N \sin \mu_n + 2\mu_n \cos \mu_n)}{[(N/2)^2 + N + \mu_n^2][N/2 + \mu_n^2]}$$

where  $\mu_n$  is given by the transcendental equation

$$\mu_n = \cot^{-1} \left( \frac{\mu_n}{N} - \frac{N}{4\mu_n} \right). \quad (42)$$

The roots of this transcendental equation, up to  $n = 18$ , have been re-evaluated on a digital computer, and are tabulated elsewhere<sup>20</sup>. Breakthrough curves based on these equations are shown in Fig. 6, in which results obtained by Brenner<sup>3</sup> have been used to extend the low- $\theta$ --high- $N$  range. Asymptotic approximations for this problem have been given by Aris and Amundson<sup>1</sup>, and extended by Jacques and Vermeulen<sup>23</sup>.



MU.30166

Fig. 6. Breakthrough curves for bounded diffusion model.

## 2. Semi-infinite Column (Unbounded Diffusion)

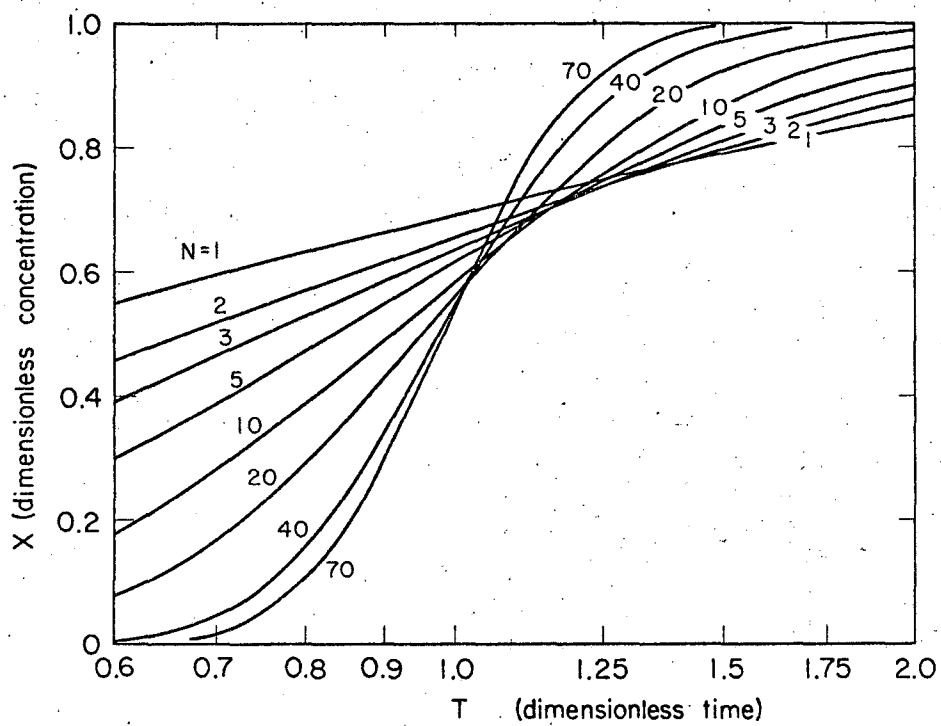
The second type of boundary condition applied to the diffusion model assumes a column of infinite length extending from  $z = 0$  to  $z = +\infty$ ; solution of uniform composition enters at  $z = 0$ , starting at  $t = 0$ , and progressively displaces the solute-free fluid initially in the column. Danckwerts has given a relation for the concentration at a point downstream, which takes the following dimensionless form:

$$X = \frac{1}{2} \left\{ 1 - \operatorname{erf} \frac{N - \theta'}{2\sqrt{\theta'}} \right\} \quad (43)$$

where  $\theta'$  is a dimensionless time ratio based on the time to reach  $X = 0.50$ . By numerical integration it is found that  $\theta'$  is  $(N + 1)U_0 t/h$ , or  $(N + 1)\theta/N$ . Hence, using  $T = \theta/N$ , Eq. (43) becomes

$$X = \frac{1}{2} \left\{ 1 - \operatorname{erf} \frac{N - (N + 1)T}{2\sqrt{(N + 1)T}} \right\} \quad (44)$$

Numerical results are given in Fig. 7. It is seen that the "unbounded" solution approaches the "bounded" curves (Fig. 6) at high  $N$ .



MU-31802

Fig. 7. Breakthrough curves for unbounded diffusion model.

#### D. Random-Walk Model

The random-walk model applies to the motion of tracer molecules traveling through the column. Their path is made up of a succession of motion and rest phases, where the motion phases require negligible time compared to the rest phase. Physically, the motion phase may correspond to the narrow void channels in a packed bed, through which the liquid moves at high velocity; whereas the rest phases will then represent the wider void spaces. Diffusion, also, could be viewed as a random-walk process of individual molecules or of fluid packets, but one occurring with equal ease in the upstream and downstream directions. The distinguishing feature of the present model is that the random walk occurs in the downstream direction only.

In the derivation the fluid is considered to travel with a characteristic velocity  $\bar{u}$ , in a series of discrete jumps corresponding to a mean free path  $l$ .<sup>5, 23</sup> For a column of length  $h$ , in which a particular portion of fluid has stayed for a time  $t$ , a number of mixing lengths  $N = h/l$  and a dimensionless time scale  $\theta' = \bar{u}t/l$  can be defined.

The analysis is based upon the probability of finding any one packet of fluid at  $N$  mixing lengths away from the inlet at time  $\theta'$ , after it has taken  $(n+1)$  jumps away from the inlet in its random walk; all possible paths for arriving at  $N$  at time  $\theta'$  are taken into account. This probability is

$$p(N, \theta') = \sum_{n=0}^{n=\infty} [\exp(-N-\theta')] \frac{N^n}{n!} \frac{\theta'^n}{n!} \quad (45)$$

This relation can be converted to a continuous function, which has the normalized form

$$p(N, \theta') d\theta' = [\exp(-N-\theta')] I_0(2\sqrt{N\theta'}) d\theta' \quad (46)$$

Here  $I_0$  is the zero-order Bessel function of the first kind with imaginary argument. If a step input of tracer is fed in continuously starting at time  $\eta = 0$ , the equation for the concentration at plane  $N$  is

$$X = \frac{c}{c_0} = \int_0^{\theta'} \exp(-N-\eta) I_0(2\sqrt{N\eta}) d\eta, \quad (47)$$

with  $X$  increasing from zero toward unity as  $\theta'$  increases toward infinity. It may be noted that  $X = 1 - J(T', N)$ , using a function  $J$  derived to describe heat and mass transfer in fixed beds.<sup>18, 22</sup> A useful simplification for Eq. (47), as developed by Klinkenberg,<sup>27</sup> is

$$X = 1/2[1 + \operatorname{erf}(\sqrt{\theta' - 1/4} - \sqrt{N + 1/4})]. \quad (48)$$

For any value of  $N$ , the stoichiometric point will occur for  $\theta = N$ . A material balance yields the result that when  $t = h/U$ , with  $U$  being the average linear velocity,  $\theta' = N + 1$ . The derivation of this important result is given in the Appendix. Through this relation, the characteristic velocity is related to the average linear velocity by the equation  $\bar{u} = U(N + 1)/N$ ; the dimensionless time becomes  $\theta' = (Ut/l) \cdot (N+1)/N$ . These considerations lead to the following definition of  $T_1$  as in Eq. (44):

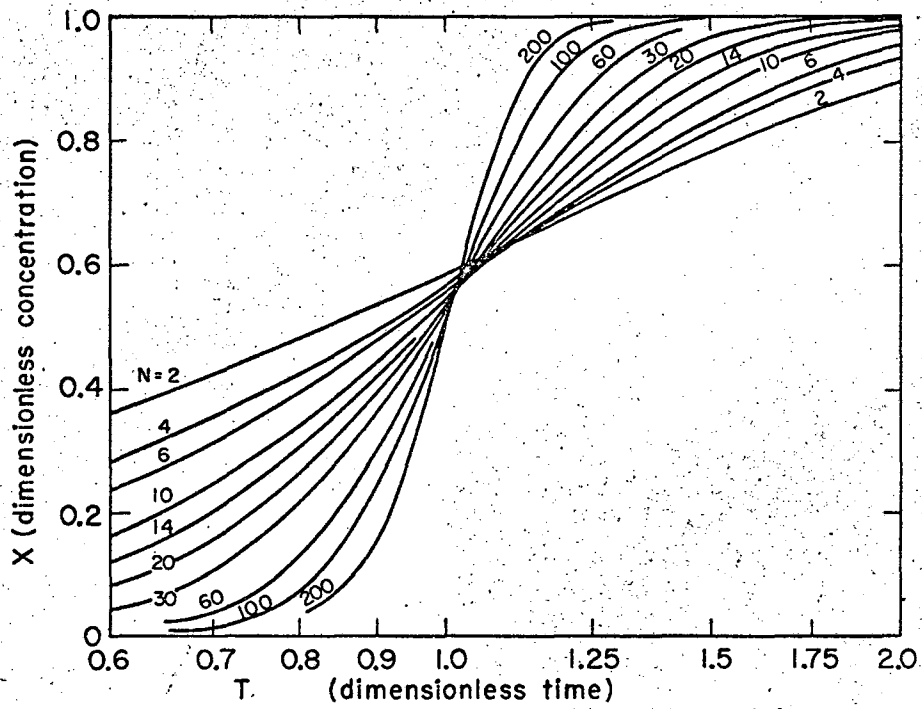
$$T = \frac{\theta'}{N} = \frac{\theta'}{N+1}. \quad (49)$$

Also, evidently, we have  $\theta \equiv Ut/l = \theta' N/(N+1)$ .

With these definitions, the Klinkenberg approximation becomes

$$X = 1/2\{1 + \operatorname{erf}[\sqrt{(N+1)T - 1/4} - \sqrt{N+1/4}]\}. \quad (50)$$

Values of  $X$  for different values of  $T$  and  $N$  computed from Eq. (50) are given in Fig. 8.



MU-30170

Fig. 8. Breakthrough curves for the random-walk model.

An eddy-dispersion coefficient  $E$  and a Péclet number  $P$  for the random-walk model are defined by comparison with the diffusion model:

$$E = U_0 \ell, \quad (51)$$

and

$$P \equiv \frac{d_p}{\ell} = \frac{d_p U_0}{E} \quad (52)$$

Consistent with this, we have  $N \equiv h/\ell = Ph/d_p = hU_0/E$ .

### E. Mixing-Cell Model

Kramers and Alberta,<sup>29</sup> followed by other investigators,<sup>1, 6, 7, 33</sup> proposed that the mixing effects occurring in process equipment could be described in terms of a cascade of mixing cells. In packed columns, the voids between the packing particles can be considered as unit cells for such mixing, the influent to a cell acting as a jet which sustains a mixing condition. At high Reynolds-number values, well within the turbulent-flow regime, the individual voids may each approach perfect mixing. Even if local mixing is not complete, a series of voids may be represented theoretically by a mixing cell.

In each "cell" perfect mixing is assumed to occur, such that the effluent from the cell has the same composition as the fluid at all points within the cell. For a step-function feed of a tracer solute (at concentration  $c_0$ ) at the inlet to a sequence of mixing cells of equal size, the effluent from the  $N$ th cell in the series has the dimensionless concentration

$$X_N = 1 - \left[ 1 + \tau + \frac{1}{2!} \tau^2 + \cdots + \frac{1}{(N-1)!} \tau^{N-1} \right] e^{-\tau} \quad (53)$$

in terms of total elapsed time  $t$ , with  $\tau = t/\bar{t}$ , where  $\bar{t}$  is the average residence time in the sequence.

The mixing-cell model is identical with a random-walk process in which the time for each step is variable, but the step length is fixed. The probability of encountering a tracer molecule in the outflow from the  $N$ th cell, at a time  $t$  after it has entered the first cell, is

$$p(N, \tau) = \frac{e^{-\tau} \tau^N}{N!} \quad (54)$$

Integrating with respect to time, from  $\tau = 0$  to  $\tau$ , leads to Eq. (53).

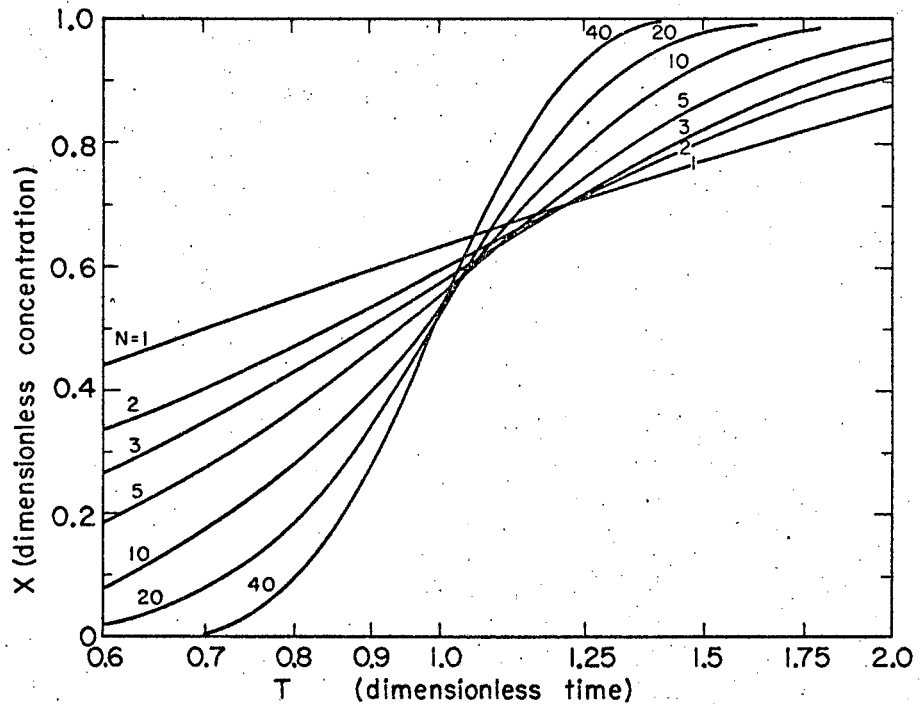
By comparing the diffusion model and the mixing-cell model, several investigators for one-phase<sup>1, 29, 33</sup> and two-phase studies<sup>30, 35</sup> have shown that the cell size in the mixing-cell model corresponds to twice the mixing length in the diffusion model. This comparison can be most easily seen by using the finite-difference form of the diffusion equation. The diffusion equation has the form

$$\ell \frac{\Delta_2 X}{(\Delta z)^2} - \frac{\Delta X}{\Delta z} - \frac{\epsilon}{U_0} \frac{dX_N}{dt} = 0, \quad (55)$$

where  $\Delta X$  and  $\Delta_2 X$  stand for the first and second differences, evaluated at plane  $N_D$ . We now adopt  $\Delta z = 2\ell$  ( $=2d_p/P$ ). For this interval the function of  $X_{N-1}$ ,  $X_N$ , and  $X_{N+1}$  reduces solely to a function of  $X_{N-1}$  and  $X_N$ . The mixing-cell equation likewise involves a function of  $X_{N-1}$  and  $X_N$ , which is found to be the same function. The weak point in the match is in the initial adoption of the finite-difference form; this is valid only if  $\Delta z \ll h$ , or hence if  $N$  ( $=h/\ell$ ) is large.

If every void in a packed bed were to be a perfect mixer, we would have  $\lambda \approx 0.8 d_p$ , and  $P \sim 2.5$ . Experimentally, values of  $P$  from 0.4 to 2.3 are encountered for single-phase flow, with the lower values occurring in laminar flow.

Concentration--time curves for the mixing-cell model, computed from Eq. (53), are shown in Fig. 9. Here the dimensionless time  $T$  is  $t/NE$ .



MU-30164

Fig. 9. Breakthrough curves for the mixing-cell model.

### F. Relations Between the Different Models

Chemical-engineering interest in axial dispersion, up to the present, has centered upon fluid mixing in the turbulent (or nearly turbulent) flow regime. In this region, the diffusion, random-walk, and void-cell-mixing models are nearly equivalent, and all appear to give consistent descriptions of the experimental results. The analysis of liquid-liquid extraction in packed columns places new emphasis on the interpretation of longitudinal-dispersion behavior in laminar flow. From a theoretical viewpoint the void-cell mixing model cannot apply to this region, at least for liquids, owing to the fact that perfect mixing no longer is approached in each void cell. The diffusion model with finite boundary conditions and the random-walk model, as empirical treatments, may apply relatively well to all flow conditions. Clearly the segmented-laminar-flow model, with an appropriate velocity profile, is applicable only to the laminar-flow regime. For the most part, the step responses given by the different models do not coincide over their entire rise. Quantitative comparison hence has to be made at some reference condition; this is selected here as the (dimensionless) midpoint slope. A plot of dimensionless slopes for the different models, as functions of  $N$ , is given in Fig. 10. This figure shows that, for small slopes, the use of one or the other model to analyze experimental data can easily lead to  $N$  values (or to packing Péclet numbers) differing by a factor of two.

The finite-boundary diffusion model and the random-walk have similar midpoint-slope values. The entire breakthrough curves given by the two models have quite similar shapes, with the result that the  $t_{50}$  values for the diffusion model are only about 2% less than those for random walk.

The midpoint slopes can be expressed in a convenient form by the following empirical relations, where  $s \equiv dX/d(t/t_{50})$ :

$$\text{Mixing cell, } N_c = 2\pi s^2 + 0.25$$

$$\text{Unbounded diffusion, } N_{ud} = 4\pi s^2$$

$$\text{Bounded diffusion, } N_{bd} = 4\pi s^2 - 1.45$$

$$\text{Random walk, } N_{rw} = 4\pi s^2 - 0.80$$

$$\text{S.l.f. -quartic, } N_{sq} = 4\pi s^2 - 6.0$$

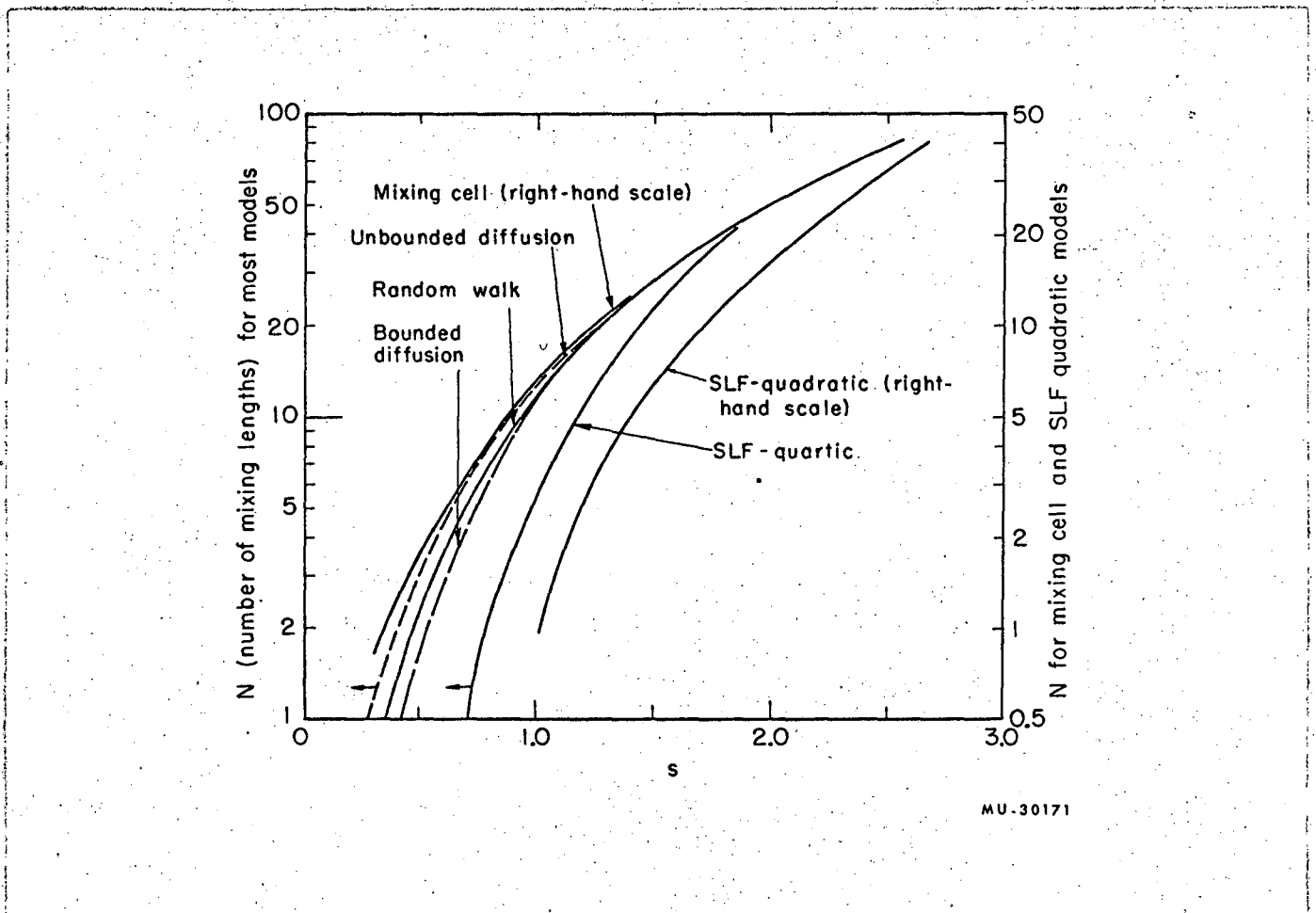


Fig. 10. Midpoint slopes for different models.

The segmented-laminar-flow result with a quartic velocity distribution approaches the diffusion model at large values of  $N$ ; in the low- $N$ -value range, at any given  $N$ , it predicts less axial dispersion than the preceding models. The segmented-laminar-flow result with quadratic velocity profile (not recommended for use) seems to indicate that, for large  $N$ 's,  $N_{SFP}$  approaches  $N_D/2$ .

For reference purposes the unbounded-diffusion results are also shown, which for large  $N$  values become equivalent to the diffusion model with finite boundary conditions. The void-cell model at high  $N$  is approximately equivalent to the diffusion model (with  $N_c \approx N_D/2$ ). At low  $N$ 's it approximates the unbounded diffusion model.

In the low- $N$  (shallow-bed) range the difference between the diffusion model and the segmented-laminar-flow model (quartic) is quite large. For a few experimental studies of laminar-flow dispersion, the diffusion model (or the nearly equivalent random-walk model) has been found to give a much more constant value of packing Péclet number for different bed heights<sup>23</sup>. Hence the quartic velocity distribution we have used does not represent adequately the actual flow behavior in sphere- and ring-packed beds. A different velocity distribution, or a more detailed statistical treatment of fluid-filament behavior, may perhaps lead to a satisfactory fit.

G. Notation

- c Concentration.  
 $c_b$  Flow average concentration.  
 $c_0$  Feed concentration.  
  
 $d_p$  Particle diameter.  
 E Longitudinal-dispersion coefficient, based on superficial velocity,  $U_0 l$ .  
 erf Error function;  $\frac{2}{\sqrt{\pi}} \int_0^X e^{-x^2} dx$ .  
  
 f Friction factor.  
 $f(t)$  Dimensionless function of time.  
  
 h Total height of bed.  
 $h'$  Modified height of bed =  $(N-1)h/N$ .  
 H Heaviside unit function.  
 i Integer.  
 $I_0$  Bessel function of zero order, with imaginary argument.  
 $j_d$  Colburn j factor, for mass transfer.  
 J Function used in regenerative heat and mass transfer operations.  
  
 $l$  Mixing length.  
 $m, m'$  Integers.  
 n Number of random-walk jumps under consideration.  
 N Number of dispersion units (mixing lengths), laminar-flow segments, or mixing cells.  
 $N_{Re}$  Reynolds number,  $U_0 d_p / \nu$ .  
 p Probability.  
 P Péclet number,  $d_p / l$ .  
 r Radial coordinate.

- $\vec{r}$  Radius vector.
- R Total radius.
- s Dimensionless midpoint slope (based on  $t/t_{50}$  scale).
- S Cross-section.
- t Time.
- $t_1$  Time defined by Eq. (3).
- $\bar{t}$  Residence time.
- T Dimensionless time,  $\theta/N$ .
  
- u Characteristic, or local, velocity in segmented laminar-flow model.
- $\bar{u}$  Characteristic velocity in random-walk.
- $u_{\max}$  Maximum velocity.
- U Interstitial velocity or mean linear velocity.
- $U_0$  Superficial velocity;  $\epsilon U$ .
- $U_\infty$  Asymptotic uniform velocity of fluid past a single sphere.
- V Variable defined in Eq. (36).
- W Variable defined in Eq. (30).
- X Dimensionless concentration;  $c/c_0$ .
- z Axial distance.
- Z Dimensionless length;  $z/h$ .
- $\alpha$  Dimensionless time ;  $\Theta/(\Theta+1)$ .
- $\delta$  Time increment.
- $\epsilon$  Void-fraction.
- $\zeta$  Variable defined by Eq. (9), ( $\zeta=1-r^2/R^2$ ); fraction of cross-section enclosed between r and R.
  
- $\xi$  Dummy variable.
- $\eta$  Dummy variable.
- $\mu_n$  Roots of transcendental equation [ Eq. (45) ] .
- $\nu$  Kinematic viscosity.
- $\tau$  Time variable.
- $\theta$  Dimensionless time,  $Ut/l$ .
- $\theta'$  Dimensionless time,  $\bar{u} t/l$ .

References

1. R. Aris and N. R. Amundson, A. I. Ch. E. J. 3, 280 (1957).
2. R. B. Bird, W. E. Stewart, and E. N. Lightfoot, Transport Phenomena, (John Wiley and Sons, Inc., New York, 1960), p. 297, 641.
3. H. Brenner, Chem. Eng. Sci. 17, 229 (1962).
4. P. C. Carman, Trans. Inst. Chem. Engrs. (London) 15, 150 (1937).
5. E. J. Cairns and J. M. Prausnitz, Chem. Eng. Sci. 12, 20 (1960).
6. J. J. Carberry, A. I. Ch. E. J. 4, 13M (1958).
7. J. J. Carberry and R. H. Bretton, A. I. Ch. E. J. 4, 367 (1958).
8. H. S. Carslaw and J. C. Jaeger, Conduction of Heat in Solids, (Oxford University Press, England, 1959); 2nd ed., pp. 114-119.
9. F. E. Crane and G. H. F. Gardner, "Measurements of Transverse Dispersion in Granular Media," Technical Report from Gulf Research and Development Co., Pittsburgh, Pa. April 18, 1960.
10. P. V. Danckwerts, Chem. Eng. Sci. 2, 1 (1953).
11. J. F. Davidson, E. J. Cullen, D. Hanson, and D. Roberts, Trans. Inst. Chem. Engrs. (London) 37, 122 (1959).
12. H. A. Deans, A. I. Ch. E. J. 9, 106 (1963).
13. P. F. Deisler and R. H. Wilhelm, Ind. Eng. Chem. 45, 1219 (1953).
14. W. Eguchi, Chem. Eng. (Japan), 26, 947 (1962).
15. H. A. Einstein (Ph. D. Dissertation), Eidg. Techn. Hochschule, Zürich (1937).
16. B. W. Gamson, Chem. Eng. Progr. 47, 19 (1951).
17. F. H. Garner, V. G. Jenson, R. B. Keey, Trans. Inst. Chem. Engrs. 37, 191 (1959).
18. S. Goldstein, Proc. Roy. Soc. (London) A219, 151 (1953).
19. C. F. Gottschlich, A. I. Ch. E. J. 9, 88 (1963).
20. A. Hennico, G. L. Jacques, and T. Vermeulen, Lawrence Radiation Laboratory Report UCRL-10697 (1963).

21. J. W. Hiby, Proceedings, Symposium on Interaction between Fluids and Particles (Instn. Chem. Engrs., London, 1962), pp. 312-325.
22. N. K. Hiester, and T. Vermeulen, Chem. Eng. Progr. 48, 505 (1952).
23. G. L. Jacques, and T. Vermeulen, University of California Radiation Laboratory Report UCRL-8029, (1958); paper submitted.
24. G. L. Jacques, J. E. Cotter, and T. Vermeulen, University of California Radiation Laboratory Report UCRL-8658 (1959).
25. M. Jakob, Heat Transfer, 1 (John Wiley and Sons, Inc., New York, 1949), p. 424.
26. G. de Josselin de Jong, Trans. Amer. Geophys. Union 39, 67 (1958).
27. A. Klinkenberg, Ind. Eng. Chem. 46, 2285 (1954).
28. V. Koump. (D. EngThesis) Yale Univ. (1959).
29. H. Kramers and G. Alberta, Chem. Eng. Sci. 2, 173 (1953).
30. G. A. Latinen (Ph. D. Thesis), Princeton Univ. (1954).
31. O. Levenspiel and W. K. Smith, Chem. Eng. Sci. 6, 227 (1957).
32. I. I. Martin, W. W. McCabe, and C. C. Monrad, Chem. Eng. Progr. 47, 91 (1951).
33. K. W. McHenry and R. H. Wilhelm, A. I. Ch. E. J. 3, 83 (1957).
34. T. Miyauchi, University of California Radiation Laboratory Report UCRL-3911 (1957).
35. T. Miyauchi, and T. Vermeulen, Ind. Eng. Chem. Fundamentals 2, <sup>113</sup> (1963).
36. W. E. Ranz, Chem. Eng. Progr. 48, 247 (1952).
37. P. G. Saffman, J. Fluid Mech. 6, 321 (1959); Chem. Eng. Sci. 11, 125 (1959); J. Fluid Mech. 7, 194 (1960).
38. C. A. Sleicher, A. I. Ch. E. J. 5, 145 (1959).
39. D. A. Strang and C. J. Geankoplis, Ind. Eng. Chem. 50, 1305 (1958).
40. G. I. Taylor, Proc. Roy. Soc. (London) A219, 186 (1953); *ibid.* A223, 446 (1954); *ibid.* A225, 473 (1954).
41. J. F. Wehner and R. H. Wilhelm, Chem. Eng. Sci. 6, 89 (1956).
42. S. Yagi and T. Miyauchi, Chem. Eng. (Japan) 17, 382 (1953).

Appendix

Determination of Stoichiometric Time for the Random-Walk Model

The stoichiometric time is defined as the time necessary to fill one column volume with fluid. Usually a time scale  $T$  is adopted such that the stoichiometric time corresponds to  $T = 1$ . From a material balance, this is equivalent to choosing a time scale such that the area between the breakthrough curve ( $X$  vs  $T$ ) and the horizontal line corresponding to  $X = 1$  is equal to unity.

The general equation for the random-walk model is

$$X(\theta', N) = \int_0^{\theta'} e^{-(N+\eta)} I_0(2\sqrt{N\eta}) d\eta \quad (1)$$

with  $X(\infty, N) = 1$ . The area, mentioned above, which should be 1 is

$$\begin{aligned} S(N) &= \int_0^{\infty} [1 - X(\theta', N)] d\theta' \\ &= \int_0^{\infty} d\theta' \int_{\theta'}^{\infty} e^{-(N+\eta)} I_0(2\sqrt{N\eta}) d\eta. \end{aligned} \quad (2)$$

Integrating by parts leads to

$$\begin{aligned} S(N) &= \left[ \theta' \int_{\theta'}^{\infty} e^{-(N+\eta)} I_0(2\sqrt{N\eta}) d\eta \right]_0^{\infty} \\ &\quad + \int_0^{\infty} \eta e^{-(N+\eta)} I_0(2\sqrt{N\eta}) d\eta. \end{aligned} \quad (3)$$

We first show that

$$\left[ \theta' \int_{\theta'}^{\infty} e^{-(N+\eta)} I_0(2\sqrt{N\eta}) d\eta \right]_0^{\infty} = 0 \quad (4)$$

This expression can be simplified by the following change of variable:

$$\xi = 2\sqrt{N\eta}; \text{ then } \eta = \xi^2/4N, \text{ and } d\eta = (\xi/2N) d\xi.$$

Equation (53) becomes

$$\left[ \theta' \frac{e^{-N}}{2N} \int_{2\sqrt{N\theta'}}^{\infty} e^{-\xi^2/4N} I_0(\xi) \xi d\xi \right]_0^{\infty} = 0. \quad (5)$$

We first note that the expression under the integral is always positive and that the function  $I_0(\xi)$  satisfies the inequality

$$I_0(\xi) < e^{\xi} \quad (6)$$

for all positive values of  $\xi$ . From this, the expression between brackets clearly vanishes when  $\theta' = 0$ . To show that the same expression is zero at the upper limit, the expression will be replaced by a simpler and larger function which tends to zero when  $\theta' \rightarrow \infty$ . Using Eq. (6) we can write

$$e^{-\frac{\xi^2}{4N}} I_0(\xi) < e^{-\frac{\xi^2}{4N} + \xi} < e^{-\xi} \quad (7)$$

for all  $\xi > \xi_1$ . Note that this relation holds for  $\xi_1 > 8N$ . Then, we have

$$\int_{2\sqrt{N\theta'}}^{\infty} e^{-\frac{\xi^2}{4N}} I_0(\xi) \xi d\xi < \int_{2\sqrt{N\theta'}}^{\infty} e^{-\xi} \xi d\xi. \quad (8)$$

This last integral is equal to  $(1 + 2\sqrt{N\theta'}) e^{-2\sqrt{N\theta'}}$ . Finally, Eq. (5) can be replaced by the dominating function

$$f = \theta' \frac{e^{-N}}{2N} (1 + 2\sqrt{N\theta'}) e^{-2\sqrt{N\theta'}}, \quad (9)$$

which tends to zero when  $\theta'$  tends toward  $\infty$ . As the expression between brackets in Eq. (5) is always positive and smaller than  $f$ , it also vanishes for  $\theta' \rightarrow \infty$ . Now, the area is given by

$$S(N) = \int_0^{\infty} \eta e^{-(N+\eta)} I_0(2\sqrt{N\eta}) d\eta. \quad (10)$$

Using the same change of variable as above, Eq. (10) becomes

$$S(N) = e^{-N} \frac{1}{2} \int_0^{\infty} \frac{\xi^2}{4N^2} e^{-\frac{\xi^2}{4N}} I_0(\xi) \xi d\xi, \quad (11)$$

or

$$S(N) = e^{-N} \frac{\partial}{\partial N} \left( \frac{1}{2} \int_0^{\infty} e^{-\frac{\xi^2}{4N}} I_0(\xi) \xi d\xi \right). \quad (12)$$

Also, Eq. (1) can be written

$$X(\theta', N) = \frac{e^{-N}}{2N} \int_0^{2\sqrt{N\theta'}} e^{-\frac{\xi^2}{4N}} I_0(\xi) \xi d\xi. \quad (13)$$

Since we have  $X(\infty, N) = 1$  when  $\theta' \rightarrow \infty$ , we get

$$\frac{1}{2} \int_0^{\infty} e^{-\frac{\xi^2}{4N}} I_0(\xi) \xi d\xi = N e^N. \quad (14)$$

Using Eq. (14) in Eq. (12) it follows that

$$S(N) = e^{-N} \frac{\partial}{\partial N} (N e^N) = N+1. \quad (15)$$

Thus, to normalize the breakthrough curves for the random-walk model, the following time scale has to be used:

$$T = \theta' / (N+1) \quad (16)$$

With this time scale, the stoichiometric time occurs for  $T = 1$ .

This report was prepared as an account of Government sponsored work. Neither the United States, nor the Commission, nor any person acting on behalf of the Commission:

- A. Makes any warranty or representation, expressed or implied, with respect to the accuracy, completeness, or usefulness of the information contained in this report, or that the use of any information, apparatus, method, or process disclosed in this report may not infringe privately owned rights; or
- B. Assumes any liabilities with respect to the use of, or for damages resulting from the use of any information, apparatus, method, or process disclosed in this report.

As used in the above, "person acting on behalf of the Commission" includes any employee or contractor of the Commission, or employee of such contractor, to the extent that such employee or contractor of the Commission, or employee of such contractor prepares, disseminates, or provides access to, any information pursuant to his employment or contract with the Commission, or his employment with such contractor.

